AIAA JOURNAL
Vol. 47, No. 3, March 2009

Incipient Cavitation Studied Under Strong Thermodynamic Effect

Jonas P. R. Gustavsson,* Kyle C. Denning,† and Corin Segal‡
University of Florida, Gainesville, Florida 32611
and
Daniel J. Dorney§
NASA Marshall Space Flight Center, Huntsville, Alabama 35801

DOI: 10.2514/1.38987

Incipient cavitation was studied under simulated cryogenic conditions on a NACA0015 hydrofoil in a tunnel filled with the perfluorinated ketone 2-trifluoromethyl-1, 1, 1, 2, 4, 4, 5, 5, 5-nonafluoro-3-pentanone. Through pressure measurements on the hydrofoil, laser-illuminated high-speed photography, and flash-illuminated photography, the extent of cavitation and the characteristic frequencies of its oscillation were studied under varying speeds in the range of 1.7–6.7 m/s and several angles of attack. The results presented in this paper are limited to a 5.1-degree angle of attack. It was found that the vapor formation was much stronger in fluoroketone than in cold-water tests at similar cavitation numbers. The formed bubbles were significantly smaller and there existed an extended speed range over which fluctuation amplitudes grew with no well-defined frequency peaks, as was observed in water.

Nomenclature

C_P	=	pressure coefficient
$C_{P,l}$	=	specific heat of the liquid phase
c	=	chord length
f	=	frequency
k	=	thermal conductivity
P	=	static pressure
Pr	=	Prandtl number of fluid ($C_{P,l} \propto /k$)
P_v	=	vapor pressure
P_0	=	stagnation pressure
P_∞	=	freestream static pressure in the test section
Re	=	Reynolds number ($U_\infty c/\nu$)
St_c	=	Strouhal number based on chord length (fc/U_∞)
U_∞	=	freestream velocity at the centerline in the test section
α	=	angle of attack
ΔH_{vap}	=	heat of vaporization
ΔT	=	local temperature depression due to thermodynamic effect
ν	=	kinematic viscosity
ρ	=	density
ρ_l	=	density of the liquid phase
ρ_v	=	density of the vapor phase
σ	=	cavitation number $[(P - P_v)/(\frac{1}{2}\rho U_\infty^2)]$
$\propto$	=	dynamic viscosity ($\rho\nu$)

I. Introduction

CAVITATION is a major concern in the design of turbopumps due to its potential to cause performance degradation, vibrations, flow unsteadiness, and erosion damage [1]. The primary parameter used to determine the presence and quality of cavitation is the cavitation number σ:

$$\sigma = \frac{P_\infty - P_v}{\frac{1}{2}\rho U_\infty^2} \tag{1}$$

As a first approximation, cavitation, the formation of vapor bubbles due to a drop in local static pressure, occurs when the cavitation number reaches $-C_P$ (i.e., when the local static pressure is equal to the fluid vapor saturation pressure). Additional factors influence cavitation onset. They include the surface tension of the fluid, which decreases the cavitation number required for incipient cavitation, and the presence of dissolved gas or other nuclei in the liquid, which tends to facilitate cavitation. Furthermore, because the saturation vapor pressure is a function of temperature, a flow- or evaporation-induced change in the local temperature greatly complicates the prediction of cavitation onset. For water near ambient conditions, the temperature change is often negligible, but for other materials, the localized cooling of the liquid phase in the vicinity of a forming vapor bubble, referred to as the thermodynamic effect, must be considered. This effect is especially pronounced in so-called *thermosensitive* fluids, which include cryogenic propellants. The temperature decrease can be estimated as $\Delta T = B\Delta T^*$, where B is the nondimensional Stepanoff factor [2], which will be discussed later, and ΔT^* is the reference temperature depression defined by

$$\Delta T^* = \frac{\Delta H_{\text{vap}}}{C_{p,l}} \frac{\rho_v}{\rho_l} \tag{2}$$

Unlike the effect of surface tension and impurities, which primarily affect incipient cavitation behavior, the thermodynamic effect only becomes important once the bubbles have grown to a certain critical size. Early in the bubble development, the thermal effect can be neglected and bubble diameter grows linearly in time, as suggested by the Rayleigh–Plesset equation. Once a critical size has been reached, the localized cooling of the fluid around the bubble decreases the growth rate to $D \sim t^{-1/2}$, as is found in boiling [1]. The bubble size at which the thermodynamic effect becomes important is proportional to $1/\Delta T^*$ [3], making it irrelevant for bubble growth in pumps using water at ambient temperature, but greatly reducing the size of bubbles seen in thermosensitive fluids.

The dimensionless B factor, which may physically be interpreted as the volume ratio between the vapor and liquid phases involved in the cavitation heat exchange, may be scaled as $B \propto Re^{0.2}Pr^{0.7}$, according to Franc et al. [4]. A discussion of different temperature-

Received 9 June 2008; revision received 10 October 2008; accepted for publication 2 November 2008.

*Postdoctoral Associate, Mechanical and Aerospace Engineering, Building MAE-A, Room 231, P.O. Box 116250. Member AIAA.
†Undergraduate Assistant, Mechanical and Aerospace Engineering, Building MAE-A, Room 231, P.O. Box 116250. Student Member AIAA.
‡Associate Professor, Mechanical and Aerospace Engineering, Building MAE-A, Room 231, P.O. Box 116250. Associate Fellow AIAA.
§Aerospace Engineer, Applied Fluid Dynamics Analysis Group. Associate Fellow AIAA.

depression models and experimental data for different geometries and fluids indicates that a valid general correlation is difficult to establish [3,5]. Billet et al. [3] attempted to determine an empirical expression of B based on several dimensionless parameters, as shown in Eq. (3):

$$B = c_0(l_{\text{cav}}/D)^{c1} Re^{c2} Fr^{c3} We^{c4} Pr^{c5} Pe \tag{3}$$

The equation is based on ogive [3] and venturi [5] cavitation experiments, where D is the diameter of the ogive or venture throat. Neglecting the impact of the Weber number (i.e., $c_3 = 0$), the following parameter values were found for a venturi: $c_0 = 0.854$, $c_1 = 0.32$, $c_2 = -1.45$, $c_4 = 1.05$, and $c_5 = -0.46$; for a zero-caliber ogive, the values were $c_0 = 1.183$, $c_1 = 0.87$, $c_2 = -1.00$, $c_4 = -0.28$, and $c_5 = -0.64$. The similar signs, with the exception of c_4, and orders of magnitude for the parameters recommended for the two different geometries suggest that the model has physical validity; however, the experimental scatter and the presence of the cavity length in the correlation may make it less reliable for predictive purposes. A further complicating factor is that for high-speed flows, such as in the liquid-nitrogen venture study by Hord [5], thermal equilibrium may not be established.

II. Thermodynamic Effects

A. Tests in Water

For practical reasons, the majority of cavitation tests have been carried out in water. It has been found that dissolved gas in the liquid may have a substantial effect on incipient cavitation through facilitating the initial growth of bubbles. The process starts on a gas kernel, which lowers the pressure depression threshold due to surface tension. Dissolved gas also appears to smooth the bubble collapse, decreasing the peak pressure as the bubble rebounds, thus weakening the impinging jet that is suspected to cause cavitation damage [6].

The NACA0015 hydrofoil has a simple geometry, yet it is representative of turbopump geometries and, as such, is frequently used in these studies. Over the years, a substantial database for cavitation behavior has been generated using this geometry. The pressure oscillations are often characterized using a Strouhal number based on chord length:

$$St_c = \frac{U_\infty f}{c} \tag{4}$$

Three different regions of oscillations, labeled modes I–III, have been identified in hydrofoil tests, as illustrated in Fig. 1. At low cavitation numbers, corresponding to mode I cloud cavitation, the spectrum is dominated by a sharp peak in the range of $0.1 < St_c < 0.2$. At higher cavitation numbers, corresponding to mode II, the literature [7–9] shows a larger range of behaviors, but there is generally a second peak at higher Strouhal numbers. Kjeldsen et al. [9] found Strouhal numbers in this regime to increase with increasing cavitation numbers, from $St_c = 0.45$ at $\sigma = 1$ to $St_c = 0.6$ at $\sigma = 1.3$, both at $\alpha = 7$ deg. It has been suggested that in this regime, the Strouhal number based on cavity length may remain constant: $St_{Lcav} \approx 0.3$ [9]. At even higher cavitation numbers, a very-low-frequency cavity oscillation, referred to as mode III, has been observed, but this peak may be attributed to facility-dependent oscillations, in which the compliance of the cavitating region gives rise to large-scale liquid redistributions in the facility: for example, through oscillations against a settling tank. Finally, note that in the data of Bramanti [8], taken with water at elevated temperature, and Gustavsson et al. [10], which uses fluoroketone at temperatures close to evaporation, intermediate modes appear, previously not reported in the literature.

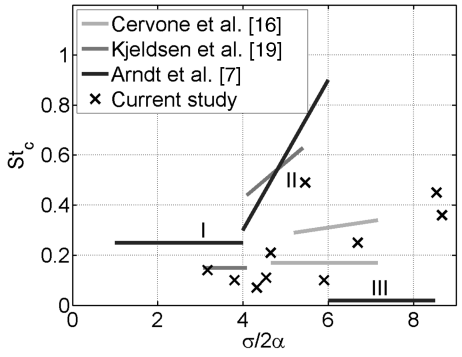

Fig. 1 Variation in Strouhal number based on dominant frequency of oscillation with angle-of-attack-corrected cavitation number for different studies. Bramanti [8], Kjeldsen et al. [9] and Arndt et al. [7] used water, whereas Gustavsson et al. [10] used fluoroketone. Modes I and II are indicated in the figure, but note that in the data of Bramanti [8], taken with elevated temperature water, and Gustavsson et al. [10], which use fluoroketone at temperatures close to evaporation, intermediate modes appear, previously not reported in the literature.

B. Tests with Substantial Thermodynamic Effect

Because of its large density ratio ρ_l/ρ_v, water exhibits a limited thermodynamic effect, or low ΔT^*, at ambient conditions. It is difficult to increase ΔT^* appreciably for water, due to the inaccessibility of the water critical point. Despite this, the thermodynamic effect has been found to reduce the breakdown cavitation number in a pump by a factor of 3 as the water temperature was increased from 20 to 140°C [6]. On the other hand, liquid hydrogen, which goes from subcritical to supercritical conditions as it passes through the low-pressure fuel turbopump in a typical engine [11], exhibits a significant thermodynamic effect. This leads to a reduction in the amount of vapor generated at a certain σ, facilitating the restart of a partially-vapor-filled turbopump and reducing the demand for a chill-down system in rocket applications [12]. Experimental studies of liquid hydrogen and nitrogen cavitation have been carried out by Hord [5], who focused on pressure measurements in a variety of geometries, and by Ruggeri and Gelder [13], who observed a substantial thermodynamic effect in liquid nitrogen as well as the frothy nature of cryogenic cavitation.

Experimentally, cryogenic propellants pose difficulties because of the need to maintain a large facility at low temperature, the presence of thermal stresses on structures and sensors, condensation and ice formation on windows, and (clearly, in the case of LH_2 or LO_2) safety issues. From a computational standpoint, the flow is challenging to simulate, because rather than having discrete vapor and liquid regions separated by a simple surface, as in water cavitation, it tends to contain extended regions of two-phase frothy mixtures. Because of their great compliance, the local speed of sound is so low, often a few meters/second, such that compressible effects, such as choking and shock waves, become important. This implies that experimental data for CFD code validation under conditions with strong thermodynamic effect are needed.

C. Present Study

To study the impact that the thermodynamic effect has on cavitation without the risks and thermal management problems imposed by handling cryogenics, this study selected 2-trifluoromethyl-1, 1, 1, 2, 4, 4, 5, 5, 5-nonafluoro-3-pentanone, hereafter referred to as *fluoroketone*, as the working fluid. It is liquid under ambient conditions, inflammable, and has a critical point of 442 K and1.87 MPa. As Table 1 shows, fluoroketone exhibits a stronger thermodynamic effect than water, even at ambient conditions, and closely matches that of hydrogen when heated to 70°C. In addition to these features, the fluoroketone also exhibits strong fluorescence with an absorption in the near UV, maximum at 305 nm, and emission in the blue region of the visible spectrum [14]. This permits the application of laser-induced fluorescence to noninvasively study the extent of the cavitating region using a 351 nm laser for excitation, as described in a previous study of developed cavitation [10]. In the present study, the focus is on incipient cavitation in a thermosensitive liquid.

Table 1 Key cavitation properties for various fluids, demonstrating the relatively strong thermodynamic effect in saturated liquid hydrogen under low-pressure turbopump inlet conditions and fluoroketone under modest temperature and pressure

Fluid	T, °C	P_v, kPa	ΔT^*, K
Water	25	3.2	0.014
	30	4.3	0.018
	50	12.4	0.050
	70	31.2	0.12
Fluoroketone	25	40.4	0.16
	70	197	1.2
Hydrogen	−250	203	1.4

III. Experimental Setup

A. Facility

A tunnel with 102×102 mm test section was constructed for these experiments and filled with the perfluorinated ketone 2-trifluoromethyl-1, 1, 1, 2, 4, 4, 5, 5, 5-nonafluoro-3-pentanone. The facility has been described in detail in [10]. Briefly, the tunnel shown in Fig. 2 is driven by a 25 hp pump and manufactured from aluminum, dimensioned to sustain pressures of up to 0.5 MPa. To reduce the amount of vapor bubbles suspended in the flow completing the loop, the stagnation chamber upstream of the test section was fitted with three fine meshes (380, 104, and 74 μm pore sizes, respectively). The tunnel is equipped with Omega PX303 pressure transducers on the stagnation chamber and collection box and a resistance temperature detector for temperature monitoring on the stagnation chamber. To reduce the amount of dissolved gas, the tunnel is connected to vacuum through a dry ice-cooled recuperation coil for a few hours before the experiments. The tunnel includes an electric heater to extend the domain of σ, but it was not used in this study.

B. Hydrofoil

A NACA0015 hydrofoil with chord $c = 50.8$ mm and a 102 mm span was used in this study. It was fitted with pressure taps at $x/c = 0.00, 0.06, 0.11, 0.17, 0.21, 0.32$, and 0.88 along the suction-side centerline. Each tap is connected to a 200 kPa (30 psia) Omega PX303 pressure transducer using tubing that was filled with liquid fluoroketone before testing to ensure a fast response.

IV. Results

A. Flash Exposure Images

Top- and side-view images of the bubble formation on the hydrofoil suction side were taken to provide a general overview of the flow. Illumination was provided using a photo flash unit with millisecond duration that ensured near-frozen flow. The top-view images in Fig. 3 show vapor formed very close to the leading edge of the hydrofoil. They indicate the growth of the cavitating region and its thickness as the speed is increased from 5.2 to 6.7 m/s. At 5.2 m/s, only a few fine bubble streaks are seen, but at 6.7 m/s, vapor covers much of the hydrofoil surface with attached bubbles upstream transforming into lifted-off clouds downstream of $x/c = 0.2$. Figure 3 also shows the small size, under 0.1 mm, of the bubbles formed in the fluoroketone even under ambient conditions, in contrast to the much larger, over 1 mm, bubbles seen in water under similar conditions [15,16].

B. High-Speed Images

Using a Photonics Industries DC10-351 laser modified to provide 527 nm output, a laser sheet was produced using fused silica lenses and a system of mirrors that allowed the sheet to project through the test-section top and front windows. The 527 nm pulse energy in the repetition-rate range of interest, 2–3 kHz, was 35 μJ. Images were recorded with a Cooke pco.1200 s camera matching the repetition

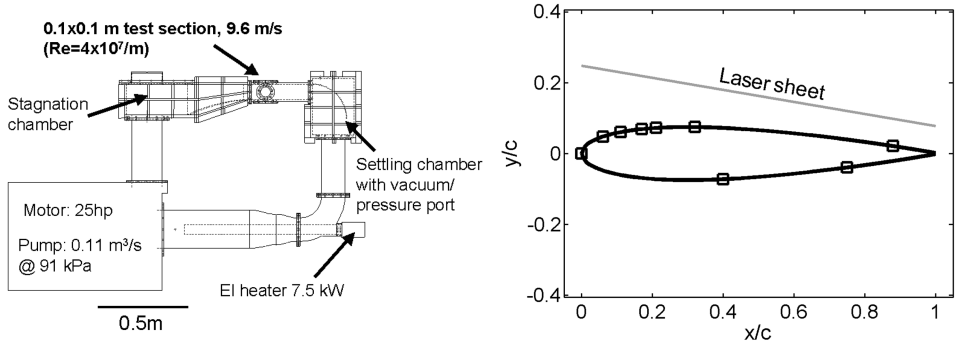

Fig. 2 Experimental layout: a) sketch of the water tunnel used in the experiments and b) NACA0015 hydrofoil with pressure ports indicated by squares and the orientation of laser sheet used for top-view high-speed images shown.

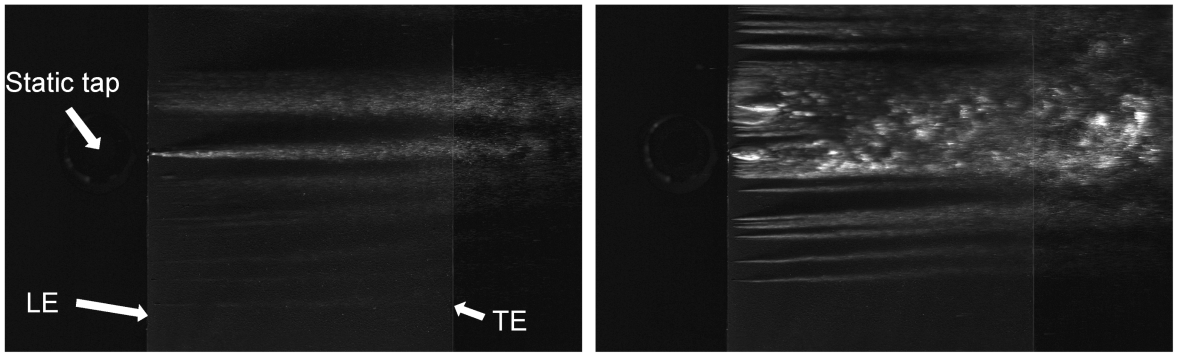

Fig. 3 Top-view flash exposure images at $\alpha = 5.1$ deg: 5.2 m/s (left) and 6.7 m/s (right). Flow is from left to right. Positions of the hydrofoil leading and trailing edges are indicated, as well as the location of the test-section static tap on the test-section floor. The images show how the incipient cavitation at 5.2 m/s gives way to more extensive developed cavitation at 6.7 m/s.

rates of the laser. The camera was fitted with a Navitar 50 mm/0.95 lens used at an aperture of $f1.4$ and directed toward the center of the hydrofoil perpendicular to the laser sheet. A series of consecutive images were taken at varying tunnel speeds through both the front and the top windows, revealing the instantaneous extent of cavitation frozen by the laser's 36 ns pulse width. Comparing the sequences taken at 5.2 m/s, shown in Fig. 4, and 6.7 m/s, shown in Fig. 5, a significant change in the amount and unsteadiness of cavitation can be seen. At 5.2 m/s, corresponding to a cavitation number of 2.78, the vapor-containing region constitutes a thin layer that remains close to the hydrofoil surface. When the speed is increased to 6.7 m/s and the cavitation number is lowered to 2.26, the vapor region grows several times in thickness, the scattering is strengthened, and the vapor-containing region varies greatly in thickness over time and space, with intermittent millimeter-size structures being convected downstream. The front portion of the cavitating region near $x/c = 0.15$ appears fairly steady over time, even at 6.7 m/s.

The top-view images shown in Figs. 6 and 7 were produced by passing a laser sheet through the front test-section window, aligning it with the trailing half of the hydrofoil suction side, and locating it 4 mm above the hydrofoil, as shown in Fig. 2b. This allowed thick vapor structures protruding through the sheet to be imaged by the high-speed camera taking images through the test-section top window at 2440 frames/second. Note that the series have been individually intensity-scaled for clarity, with the 5.2 m/s images shown in Fig. 6 amplified greatly to reveal a thin streak of bubbles similar to that seen in Fig. 3, which is only illuminated by scattered light from the sheet. The signal in Fig. 7 is 50 times stronger and results from direct scatter of the laser sheet, revealing a thicker and more unsteady vapor layer with a 4-mm-diam cloud of bubbles moving through the images close to the centerline in the presented series of images.

C. Pressure Measurements

The pressure measurements presented in Fig. 8 were obtained after degassing the fluoroketone. As Fig. 8a shows, cavitation, which occurs gradually on the hydrofoil as the tunnel speed is increased,

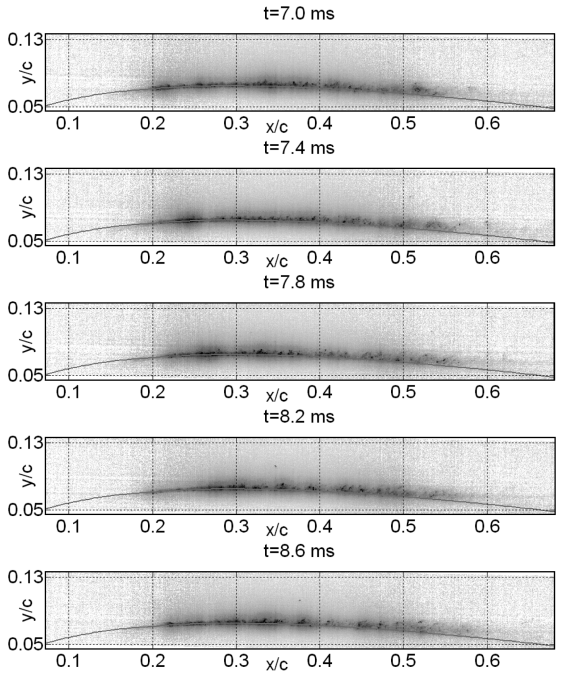

Fig. 4 Sequence of instantaneous side view images taken at 5.2 m/s and 2440 frames/second. The images have been background-corrected, and sheet nonuniformities have been corrected for over the central range of $0.19 < x/c < 0.57$. The image has been inverted and its contrast lowered for clarity. The NACA0015 hydrofoil profile is overlaid for reference.

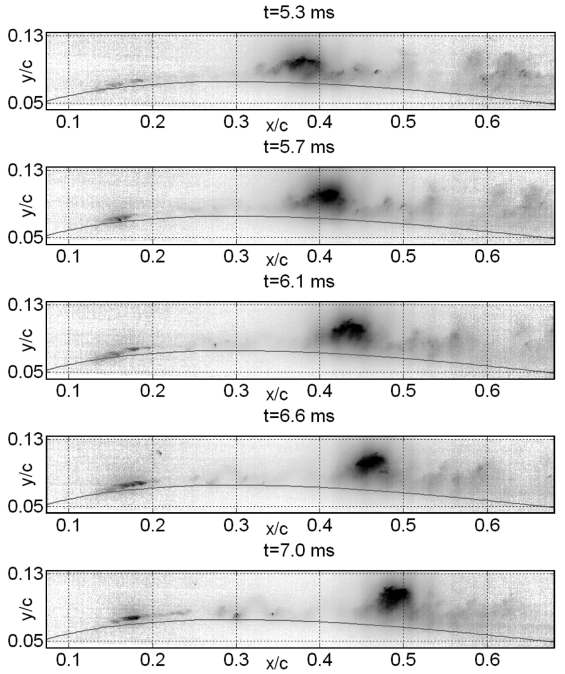

Fig. 5 Instantaneous side view images taken at 6.7 m/s at 2440 frames/second. The images have been background-corrected, and sheet nonuniformities have been corrected for over the central range of $0.19 < x/c < 0.57$.

leads to a decrease in the maximum suction peak and the formation of a longer region of more moderately adverse pressure gradient. As noted in the previous section, bubble formation was already seen at 5.2 m/s, but Fig. 8a shows that this does not affect the average pressure coefficient. At higher speeds, but well before the cavitation number has decreased below $(-C_P)_{\min}$ (e.g., $\sigma = 2.44$, and at $x/c = 0.06$, $C_P = -2.12$ at 6.7 m/s), the suction peak is reduced. Although the suction peak becomes less spiked, it also becomes longer as the cavitation number is decreased. C_P approaches a

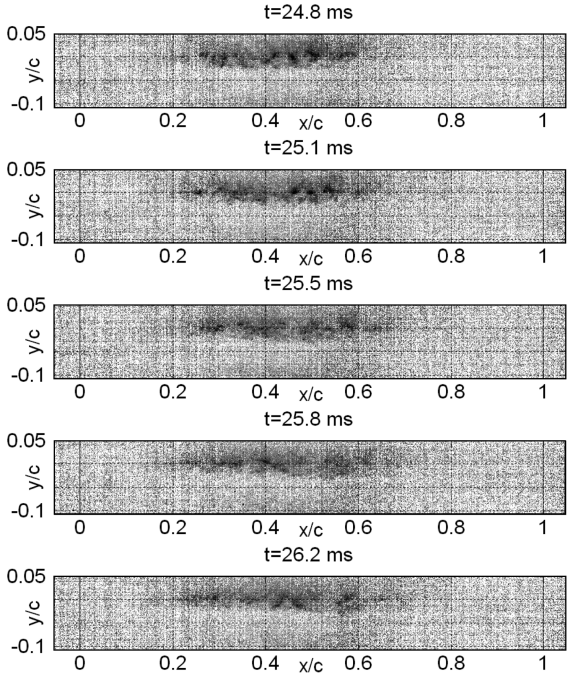

Fig. 6 Sequence of instantaneous top-view images taken at 5.2 m/s and 2786 frames/second. The images have been background-corrected, and sheet nonuniformities have been corrected for over the central range of $0.30 < x/c < 0.55$. The image contrast has been lowered for clarity. The leading and trailing edges are indicated at stations 0 and 1.

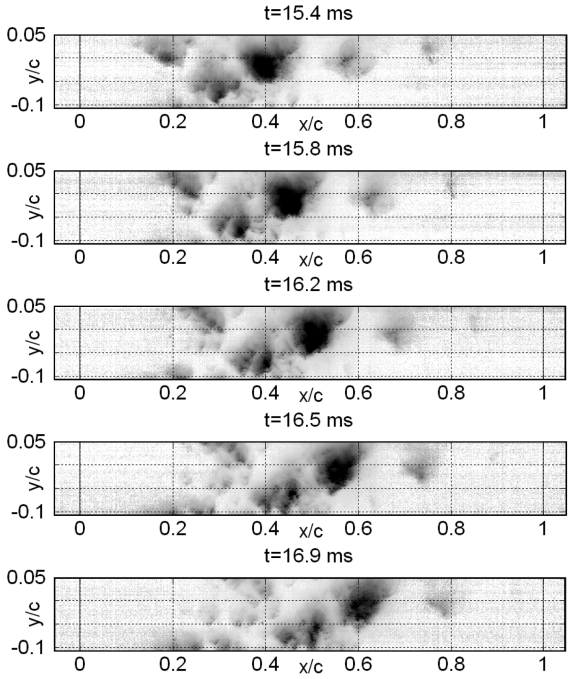

Fig. 7 Sequence of instantaneous top-view images taken at 6.7 m/s and 2786 frames/second. The images have been background-corrected, and sheet nonuniformities have been corrected for over the central range of $0.30 < x/c < 0.55$.

plateau, but still exhibits some recovery in a downstream direction, even at the lowest cavitation numbers. This is similar to the observations by Tani and Nagashima [17] in the presence of strong thermodynamic effect, but different from the results in water by Bramanti [8], where a flattening of the pressure coefficient is observed for steady cavitation.

As indicated in Fig. 8b, the change is also associated with a gradual increase in broadband pressure-fluctuation amplitude in the test section. As Fig. 8b shows, the distinct blade-passing frequencies of the pump are detected (e.g., 60 Hz at 5.2 m/s and 80 Hz at 6.7 m/s). No other individual frequencies are observed, which is similar to the observations in heated water [9].

D. Measurement Uncertainties

The pressure measurements have an uncertainty of 1.2%. The test-section static-pressure measurement has a total uncertainty of 0.7%. The pressure response-time measurements indicated a time constant of 20 ms (i.e., $1/e$ oscillations damping at 50 Hz) and a pumping pressure shift of 14 kPa during the test. The direct-connect PCB Piezotronics, Inc., transducer exhibited significantly better response with negligible damping over the frequency region studied and a negligible pumping effect. Because of the large range of dynamic pressures used in the C_P calculations, from 2.3 kPa at 1.7 m/s to 59 kPa at 8.6 m/s, the uncertainty in C_P decreases from 1.2 to 0.05% as the speed increases from 1.7 to 8.6 m/s.

V. Discussion

A. Vapor Formation

In the present experiments, vapor was found to form under conditions in which the recorded average pressures remained well above the vapor pressure at the freestream temperature, suggesting an inverse thermodynamic effect when it comes to the visual extent of cavitation compared with water tests. This trend was also observed by Bramanti [8] for water temperatures in the 25–70°C range. Taking $\sigma_i = 3.10$ and $\alpha = 5.1$ deg as the incipient conditions, we get $\sigma_i/2\alpha = 17.4$, which can be compared with the incipient threshold of 8.5 suggested by Arndt et al. [7] for NACA0015 in water. At 6.7 m/s, larger-scale cavitation with an attached upstream sheet of a typical length of $l_{\text{cav}}/c = 0.1$, varying greatly in time and across the span, is seen in Fig. 3. This corresponds to $\sigma_i/2\alpha = 13.7$, well above the value of 7.7 interpolated from the data of Arndt et al. for a cavitation bubble of this size in water, indicating that similar vapor formation is observed at higher cavitation numbers in thermosensitive liquids than in cold water.

B. Average Pressures

Studying the time-averaged pressure coefficients presented in Fig. 8 and comparing to the C_P profiles for NACA0015 profiles under noncavitating conditions given, for example, by Bramanti [8], it may be seen that the profiles here for $\alpha = 5.1$ deg and $U_\infty \leq 5.2$ m/s closely approximate the experimental results at 6 deg in water. Given an angle-of-attack uncertainty of under 0.5 deg, the explanation must be sought elsewhere. Bramanti quantified the effect due to blockage through a comparison between his experimental data using a hydrofoil with a chord length of 115 mm and a test-section height of 120 mm with theoretical pressure coefficients in unconstrained flow at 4, 5, and 6 deg. Interpolating between his pressure ports, it is found that at $x/c = 0.11$ and 0.32, the increase in $-C_P$ due to blockage is $36 \pm 2\%$. Despite half as much blockage in the present experiment, it was found necessary to increase the unconstrained $-C_P$ by 51 and 40% to achieve agreement with experimental data at $x/c = 0.11$ and 0.32, respectively. This may suggest that the pressure coefficients are affected even under noncavitating conditions by the properties of the fluid (e.g., through affecting the blockage correction). One responsible mechanism could be the increased compliance of the fluid when even minute vapor bubbles are present, resulting in a local speed-of-sound drop and a Prandtl–Glauert-like increase in $-C_P$ as well as a downstream shift of the suction peak due to compressibility effects [18]. The same effect is expected in cryogenics.

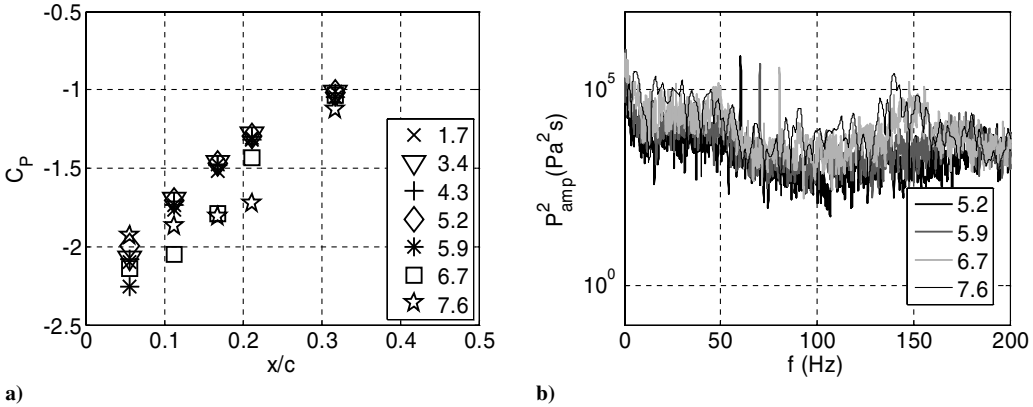

a) b)

Fig. 8 Average pressure and pressure fluctuations along the hydrofoil: a) pressure coefficient profiles and b) fluctuation spectra for the test-section static tap at varying speeds (meters/second) at $\alpha = 5.1$ deg; $\sigma = 3.10$ at 5.2 m/s, $\sigma = 2.69$ at 5.9 m/s, $\sigma = 2.44$ at 6.7 m/s, and $\sigma = 2.16$ at 7.6 m/s.

C. Pressure Fluctuations

In previous tests in fluoroketone in which developed cavitation behavior was studied, frequency analysis of the pressures in the test section exhibited distinct peaks with $0.07 < St_c < 0.50$ in the range of $4 < \sigma/2\alpha < 8$. This appeared to correspond to the transition region between mode I cavitation and mode II cavitation observed by Kjeldsen et al. [9] in water. In the present study, incipient cavitation was studied in fluoroketone and $\sigma/2\alpha > 12$. According to Arndt et al. [7], cavitation onset in the form of low-frequency mode III oscillations is only observed once $\sigma/2\alpha < 8.5$. In ambient-temperature water, Bramanti [8] noted the onset of bubble cavitation at $\sigma/2\alpha = 10.3$ at $\alpha = 6$ deg, but significant upstream pressure fluctuations were only noted as the cavitation number was lowered to $\sigma = 2.1$ at $\alpha = 8$ deg, corresponding to bubble/cloud cavitation at $\sigma/2\alpha = 7.5$. At this cavitation number, a fundamental frequency of 5 Hz with an associated harmonic of 10 Hz was observed, suggesting a Strouhal number based on chord length of 0.17.

Although no distinct peaks were noted in the pressure spectra in the current tests, there was a general trend toward increasing the rms of the pressure fluctuations as the cavitation number was decreased through a broadband increase in pressure fluctuations across the studied range of the spectrum. Separate response tests in which pressure oscillations of controlled frequency were introduced in the tunnel were performed to assess the response of various pressure ports. It was found that the hydrofoil taps exhibit a strongly-frequency-dependent response with a low-frequency decay of 1/10 at 15 Hz, followed by resonance peaks at 50 and 100 Hz, for which response factors of 0.1 and 0.06, respectively, were measured. For the intermediate valleys near 30 and 70 Hz, response factors of about 0.01 were found. This strong decay suggested that for spectral analysis, the direct-connect test-section static transducer would be most appropriate.

Because of the broadband nature of the pressure fluctuations detected, however, it is still possible to discuss the overall qualitative pressure-fluctuation amplitude variation between different ports and tunnel speed, as shown in Fig. 9. The plot shows that up to 5.9 m/s there is a gradual increase in fluctuation amplitude with increasing tunnel speed for all transducers, producing fluctuations that are 1.5–2 orders of magnitude above the noise floor suggested by data at a zero flow speed. Hence, the fine bubble streaks noted at 5.2 and 5.9 m/s appear to have little effect on the development of pressure fluctuations in the flow, just as no significant change was seen on the time-averaged C_P curves during incipient cavitation. As the freestream speed is increased to 6.7 m/s, the general upward trend continues for the facility-monitoring transducers and the pressure-side taps, but the fluctuations on the hydrofoil suction side change dramatically: the rms amplitude on the $x/c = 0.17$ and 0.21 taps increase by a factor of 2.5 and 5, respectively. Both up- and downstream of this region, the taps register a decreasing amplitude; down a factor of 3 at $x/c = 0.06$, a factor of 4 at $x/c = 0.11$, and a factor of 1.7 at $x/c = 0.32$. The Reynolds number at 5.9 m/s based on chord length is 9.2×10^5, suggesting turbulent flow over the relevant range of the hydrofoil. As the speed is further increased to 7.6 m/s, the rms amplitude is dramatically reduced at taps $x/c = 0.11$, 0.17, and 0.21 by factors of 2, 7, and 2, respectively, whereas the amplitude at $x/c = 0.32$ is doubled.

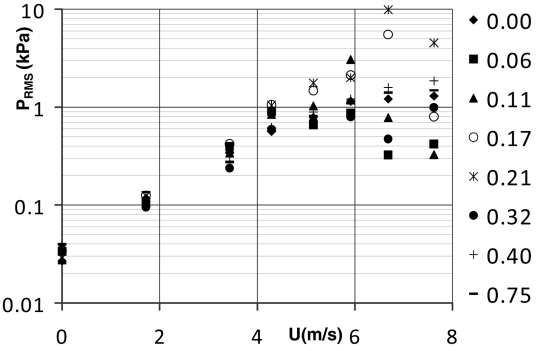

Fig. 9 Pressure fluctuation rms amplitude on various pressure taps (x/c indicated) and tunnel-monitoring pressure transducers at varying test-section freestream speeds. The figure indicates a general trend toward increasing fluctuation amplitude with increasing tunnel speed, but once cavitation occurs, several taps show a sudden decrease in pressure rms amplitude.

The fluctuation amplitude change is associated with the change in cavitation pattern observed in the images, with a larger vapor-containing region with a more persistent upstream sheet. Strong oscillations appear to be associated with the trailing edge of the attached cavitation. Comparing the fluctuation amplitudes at different speeds with the corresponding time-averaged C_P curves, strong oscillations are associated with the strong positive pressure gradient that moves downstream due to the suction peak smoothening as the cavitation number is decreased.

The pressure coefficients shown in Fig. 8 indicate that the time-averaged pressures, even at the lowest pressure post $x/c = 0.11$, is well above the saturation vapor pressure for fluoroketone. At $x/c = 0.06$, $C_P = -2.0$ at 5.2 m/s, corresponding to $P = 64$ kPa, and the vapor pressure at 25°C is 40.4 kPa. After deconvolution of the measured pressure spectra at $x/c = 0.06$ with the measured transducer response, which suggests that most energy is contained in the frequency range of less than 50 Hz, the rms fluctuation amplitude at the port is estimated at 2.8 kPa. Given that the suction peak occurs between the $x/c = 0.00$ and 0.06 ports on a NACA0015 hydrofoil at this angle of attack, using the pressure port at $x/c = 0.06$ overestimates the minimum pressure attained. Together, this suggests a mechanism whereby the fluctuations may temporarily lead to a local static pressure below the saturation vapor pressure and create vapor bubbles as seen in Figs. 4 and 6, even though the lowest time-averaged pressure is too high for this to occur.

VI. Conclusions

A study of incipient cavitation was studied under simulated cryogenic conditions on a NACA0015 hydrofoil. The results indicated the following:

1) The cavitation in fluoroketone exhibits the finer structure, which is expected of a fluid with strong thermodynamic effect such as cryogenics.

2) Visible vapor formation occurs at significantly higher cavitation numbers in a thermosensitive fluid such as fluoroketone than in water; images suggested $\sigma_i/2\alpha = 17.4$, and literature cold-water data gave $\sigma_i/2\alpha = 8.5$.

3) Fine bubble streaks seen under incipient conditions, $15.1 \leq \sigma_i/2\alpha \leq 17.4$, do not appear to affect the average pressure coefficients or the noncavitating trend toward generally increasing pressure-fluctuation amplitude as the speed is increased.

4) Further lowering the cavitation number, $12.1 \leq \sigma_i/2\alpha \leq 13.7$, greatly expanded the vapor-filled region, thickening it going downstream, and produced a more stable attached vapor region near the suction peak. In this regime, a gradual reduction in the suction peak was seen. The suction peak is also broadened, producing a weaker adverse pressure gradient and pushing it further downstream. This shift was also reflected in the fluctuation amplitudes in which large amplitudes appeared to be connected to the strong positive pressure gradient following the suction peak.

5) Frequency spectra across the studied cavitation number range, $12.1 \leq \sigma_i/2\alpha$, exhibit no sharp peaks associated with developed cavitation in water, despite the large amount of vapor present at the lowest cavitation numbers.

Acknowledgments

This work has been supported by NASA Constellation University Institute Project. We thank Claudia Meyer, Program Manager, for her support.

References

[1] Brennen, C. E., *Hydrodynamics of Pumps*, Oxford Univ. Press, Oxford, 1994.

[2] Stepanoff, A. J., "Cavitation Properties of Liquids," *Journal of Engineering for Power*, Vol. 86, No. 4, 1964, pp. 195–200.
[3] Billet, M. L., Holl, J. W., and Weir, D. S., "Correlations of Thermodynamic Effects for Developed Cavitation," *Journal of Fluids Engineering*, Vol. 103, No. 12, 1981, pp. 534–542.
[4] Franc, J.-P., Rebattet, C., and Coulon, A., "An Experimental Investigation of Thermal Effects in a Cavitating Inducer," *Journal of Fluids Engineering*, Vol. 126, No. 5, 2004, pp. 716–723. doi:10.1115/1.1792278
[5] Hord, J., "Cavitation in Liquid Cryogens," NASA CR-2156, NASA, Washington, D.C., 1973.
[6] Brennen, C. E., *Cavitation and Bubble Dynamics*, Oxford Univ. Press, New York, 1995.
[7] Arndt, R. E. A., Balas, G. J., and Wosnik, M., "Control of Cavitating Flows: A Perspective," *JSME International Journal, Series B (Fluids and Thermal Engineering)*, Vol. 48, No. 2, 2005, pp. 334–341. doi:10.1299/jsmeb.48.334
[8] Bramanti, C., Experimental Study of Cavitation and Flow Instabilities in Space Rockets Turbopumps and Hydrofoil, Ph.D. Dissertation, Univ. of Pisa, Pisa, Italy, 2006.
[9] Kjeldsen, M., Arndt, R. E. A., and Effertz, M., "Spectral Characterization of Sheet/Cloud Cavitation," *Journal of Fluids Engineering*, Vol. 122, No. 3, 2000, pp. 481–487. doi:10.1115/1.1287854
[10] Gustavsson, J. P. R., Denning, K., and Segal, C., "Experimental Study of Cryogenic Cavitation Using Fluoroketone," 46th AIAA Aerospace Sciences Meeting and Exhibit, Reno, NV, 2008.
[11] Biggs, R. E., "Space Shuttle Main Engine–The First Ten Years," *History of Liquid Rocket Development in the United States, 1955–1980*, edited by Stephen, E. Doyle, American Astronautical Society History Series, 13, Pt. 3, American Astronautical Society, Springfield, VA, 1992, Chap. 4.
[12] Bissell, W. R., Wong, G. S., and Winstead, T. W., "Analysis of Two-Phase Flow in LH_2 Pumps for O_2/H_2 Rocket Engines," *Journal of Spacecraft and Rockets*, Vol. 7, No. 6, 1970, pp. 707–713.
[13] Ruggeri, R. S., and Gelder, T. F., "Cavitation and Effective Liquid Tension of Nitrogen in a Tunnel Venturi," NASA Lewis Research Center, TN D-2088, Cleveland, OH, 1964.
[14] Gustavsson, J. P. R., and Segal, C., "Fluorescence Spectrum of 2-Trifluoromethyl-1,1,1,2,4,4,5,5,5-Nonafluoro-3-Pentanone," *Applied Spectroscopy*, Vol. 61, No. 8, 2007.
[15] Rapposelli, E., Cervone, A., Bramanti, C., and d'Agostino, L., "Thermal Cavitation Experiments on a NACA 0015 Hydrofoil," *Journal of Fluids Engineering*, Vol. 128, No. 2, 2006, pp. 326–331.
[16] Cervone, A., Bramanti, C., Rapposelli, E., and d'Agostino, L., "Thermal Cavitation Experiments on a NACA 0015 Hydrofoil," *Transactions of the ASME*, Vol. 128, No. 2, 2006, pp. 326–331. doi:10.1115/1.2169808
[17] Tani, N., and Nagashima, T., "Cryogenic Cavitating Flow in 2D Laval Nozzle," *Journal of Thermal Science and Technology*, Vol. 12, No. 2, 2003, pp. 157–161.
[18] Seifert, A., and Pack, L. G., "Oscillatory Control of Shock-Induced Separation," *Journal of Aircraft*, Vol. 38, No. 3, 2001, pp. 486–495.

F. Coton
Associate Editor